Observation of the superconducting proximity effect in Nb/InAs and NbN_x/InAs by Raman scattering

I. V. Roshchin,* A. C. Abeyta,† and L. H. Greene
Department of Physics, University of Illinois at Urbana-Champaign, 1110 West Green Street, Urbana, Illinois 61801

T. A. Tanzer,‡ J. F. Dorsten,§ and P. W. Bohn
Department of Chemistry, University of Illinois at Urbana-Champaign, Urbana, Illinois 61801

S.-W. Han** and P. F. Miceli
Department of Physics and Astronomy, University of Missouri-Columbia, Columbia, Missouri 65211

J. F. Klem
Sandia National Laboratories, P.O. Box 5800 MS 0603, Albuquerque, New Mexico 87185
(Received 25 April 2002; published 31 October 2002)

High-quality thin Nb and NbN films (60-100 Å) are grown on (100) n^+-InAs ($n=10^{19}$ cm^{-3}) substrates by dc-magnetron sputter deposition. Studies of the electronic properties of interfaces between the superconductor and the semiconductor are done by Raman scattering measurements. The superconducting proximity effect at superconductor-semiconductor interfaces is observed through its impact on inelastic light scattering intensities originating from the near-interface region of InAs. The InAs longitudinal optical phonon LO mode (237 cm^{-1}) and the plasmon-phonon coupled modes L_- (221 cm^{-1}) and L_+ (1100 to 1350 cm^{-1}), for $n^+=1\times10^{19}-2\times10^{19}$ cm^{-3} are measured. The intensity ratio of the LO mode (associated with the near-surface charge accumulation region, in InAs) to that of the L_- mode (associated with bulk InAs), is observed to increase by up to 40% below the superconducting transition temperature. This temperature-dependent change in light scattering properties is only observed with high quality superconducting films and when the superconductor and the semiconductor are in good electrical contact. A few possible mechanisms of the observed effect are proposed.

DOI: 10.1103/PhysRevB.66.134530 PACS number(s): 74.50.+r, 78.30.Fs, 63.20.−e, 73.20.−r

I. INTRODUCTION

The superconducting proximity effect occurs at a normal-metal (N)- superconductor (S) interface. The inducement of superconductivity in N and its suppression in S has been discussed as a coherent coupling of electrons and holes in N, and a pair-breaking effect in S, both produced by the Andreev reflection (AR) process.[1] In this process, an electron in the normal metal is reflected from the superconductor interface as a hole along the time-reversed path. Andreev reflection, as described by Bogoliubov–de Gennes (BdG) equations,[2] mixes electron and hole states. An equivalent description of the proximity effect is when the condensate wave function is induced in the normal metal as provided by the continuity conditions at the superconductor–normal metal (SN) interface.[3]

The strength of the proximity effect is dependent upon the transmissivity of the interface and any phase-breaking processes such as inelastic scattering. The BTK theory,[4] proposed in 1982, models the transport across such an interface using the strength of the barrier between S and N as a parameter. Such a barrier can be either due to a thin insulating layer between S and N or due to a mismatch of the Fermi velocities in S and N. Tuning the barrier strength allows for investigation of the crossover from the quasiparticle tunneling regime, where single quasiparticles, electrons, and holes tunnel across the interface, to the Andreev reflection regime. When the effective barrier is strong, i.e., in the low-transmittance regime, tunneling dominates.[4] It has been shown that the two transmission channels described by the BTK theory, quasiparticle tunneling for low-transmittance junctions and AR for high-transmittance junctions, do not account for all the transport phenomena observed, especially in the case of high-transmittance junctions.[5–7]

Our primary motivation for this work is to study the mechanism of the superconducting proximity effect in high-transmittance junctions, and also to find out if an opening of a energy gap in the density of states in the near-surface 35-Å-wide space charge region of InAs can be observed, as predicted by Volkov.[8]

We report studies of the interface between conventional superconductors Nb and NbN_x, and a highly doped semiconductor, (100)-n^+-InAs, used as N. For additional details see Ref. 9; some of this work has been reported in Refs. 10–12.

Recently, studies of superconductor-semiconductor (S-Sm) interfaces have been done by many groups around the world (see for example, the review by Kleinsasser *et al.*[13]). One of the main reasons for interest in such interfaces is that they may be used in the electronic devices, such as Josephson field effect transistors (JOFET's). These devices intrinsically operate with much lower voltages and much lower power loss than existing all-semiconductor devices.

Replacing the normal metal by a semiconductor opens several new opportunities for investigation of basic physical

properties of the *SN* interfaces. First, the electronic properties of semiconductors differ significantly from those of the metallic superconductors: Typically, the carrier concentration is 10^2-10^5 times lower, and the typical Fermi momentum and the effective mass are 10–20 times lower in a semiconductor than in a metal. Furthermore, most semiconductors form a space-charge layer at their interface. Most often, this is a depletion layer (Schottky barrier). A few narrow gap semiconductors, such as InAs, may form a charge accumulation region (CAR). The width of both the depletion and accumulation layers is determined primarily by the doping level, and the potential height is primarily determined by surface states.[14] More accurate evaluation of the size of the space charge region requires rigorous consideration of the semiconductor parameters, including the doping level, degeneracy, and actual band structure.[15] The width of the space-charge region can be modified by doping or by external electric fields that can change the effective carrier concentration and thus the band bending in the near-surface region. The height of the space-charge region can also be modified by surface treatments which affect the surface states, such as etching, metal deposition, oxidation, or chemical passivation.[16,17]

The use of a semiconductor as the normal metal allows optical methods to be employed. Even in the highly doped ($n\sim10^{19}$ cm^{-3}) semiconductors, the carrier concentration is about 2–3 orders of magnitude lower than in metals. The visible light penetration depth, determined by the skin depth, is a few hundreds of angstroms, allowing the observation of light scattering from both the near-surface space-charge layer as well as bulk lattice modes.

Raman spectroscopy has proven to be a powerful probe of the near-surface electronic structure of semiconductors.[14,18–22] Light scattering provides a measure of electron-phonon coupling in the bulk, within layers at heterostructure interfaces, and space charge layers created by surface pinning of the Fermi energy.[23] Distinct differences in the Raman-active vibrational modes of accumulated or depleted surfaces of semiconductors from those modes of the bulk are due to differences in the electronic character of the region from which scattering originates. Raman scattering is therefore an effective tool for comparison of the surface and the bulk electronic properties. It also provides information on the carrier concentration and the band bending associated with the interface. Using all these advantages, we show how Raman scattering may be used to study the influence of the normal-state and superconducting Nb and NbN films on the near-surface electronic structure of n^+-InAs.

II. EXPERIMENTAL DETAILS

A. Sample preparation

Niobium and niobium nitride films are grown in a UHV-compatible chamber by planar dc magnetron sputter deposition. Films are deposited either on a plane-parallel 0.45-mm-thick (1102)-oriented sapphire substrate or on (100)-oriented n-InAs. Two types of wafers of bulk-grown n-InAs are used. The highly Sn+S-doped n-InAs has a carrier concentration of $n=1.2\times10^{19}$ cm^{-3}, a mobility of 5.1×10^3 cm^2/V s, and a resistivity of 1×10^{-4} Ωcm as measured at 77 K. The nominally undoped InAs has a carrier concentration of $n=1.8\times10^{16}$ cm^{-3}, a mobility of 5.0×10^4 cm^2/V s, and a resistivity of 6.9×10^{-3} Ωcm as measured at 77 K. The films are parallelogram shaped, with sides 3.2 mm×11 mm at 45°, with the longer side along the (011) direction of InAs substrate, for convenience of Raman spectroscopy measurements.

To clean the substrate surface of water and hydrocarbons, an *in situ* bake at 60−100 °C is performed simultaneously with a ~30-h pumpdown. When a base pressure lower than 3×10^{-8} Torr is achieved, the Meissner trap is filled with liquid nitrogen, and the base pressure is typically reduced to below 2×10^{-9} Torr. A gentle Ar-ion etch (beam current: 1 mA, beam voltage: 75 V, 30 sec) is performed *in situ* on the InAs in order to remove the surface oxide layer, estimated to be 20–30 Å thick. Then, after a 10–20-min pumpdown, ultrahigh purity (99.999%) Ar is leaked into the system to a pressure of 7.0×10^{-3} Torr. Immediately following 10–15 min of presputtering, the shutter is opened, and the Nb film is deposited at an approximate rate of 8 Å/sec on the substrate kept at 100 °C. Some of the Nb films are sputtered at a higher Ar pressure (3.5×10^{-2} Torr) in order to reduce surface damage to the InAs.

NbN_x films are grown by reactive dc magnetron sputter deposition using the procedure similar to that for Nb films, except that a mixture of ultra-high-purity (99.999%) argon and the grade ''zero'' (99.95%) nitrogen is used during film deposition. The ratio of the flow rates of Ar and N_2 is 108:15, as optimized for the highest T_c of the NbN films. The details of these procedures are described in Ref. 9.

B. Measurement techniques

The dc resistivity measurements are done in the standard four-probe geometry. The gold wire probe leads are attached using In:Ag alloy solder. The superconducting critical temperature is determined from the temperature dependence of the resistivity, and is defined as the temperature at which the extrapolated normal-state resistivity is reduced by 50%.

The Raman spectroscopy measurements are done in a near backscattering geometry with an incidence angle of approximately 15° (Refs. 18,20,24). The $x(y,z)\overline{x}$ configuration is used primarily, where x, y, and z represent the (100), (010), and (001) directions, respectively. The first x and the last $\overline{x}$ symbols correspond to the direction of light propagation, or k vector, of the incident and detected light, respectively. The symbols inside the parentheses (y,z) correspond to the polarization of the incident and scattered light, respectively. An argon-ion laser is used in all Raman measurements at four wavelengths: 457.9, 488, 496.5, and 514.5 nm.

In order to guide the beam to the correct height and to eliminate interference from the laser plasma lines, thus avoiding any interference with the Raman spectra, a high index equilateral triangular prism is used. After going through a polarizer which defines the incident polarization, the light is focused by either a spherical or cylindrical plano-convex lens, both with a focal length of 30 cm. The former

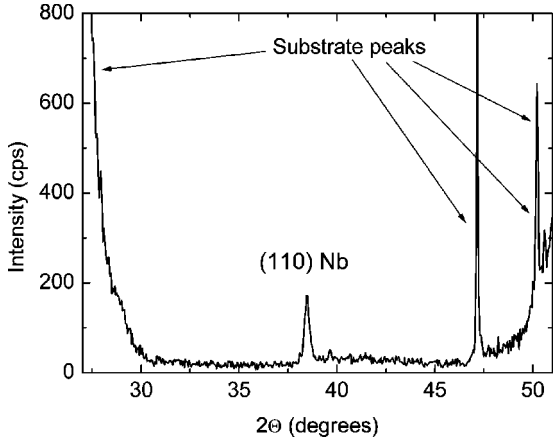

FIG. 1. X-ray diffraction: $\Theta-2\Theta$ scan for a 5700-Å-thick Nb film on sapphire. The peak at 38.46° corresponds to (110)-Nb and all other (25.58°, 47.15°, 50.20°, and 52.55°) peaks arise from the sapphire substrate.

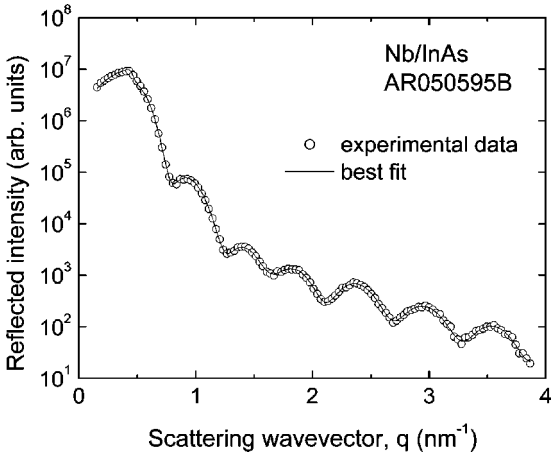

FIG. 2. X-ray reflectivity vs vector transfer $q=2k\sin\Theta$, where Θ is the incident angle of the x-ray beam, for a thin Nb film on InAs. The fit done using Parratt's method (Ref. 25), presented as a solid line, yields an InAs substrate roughness of 1.4 ± 1.0 Å, Nb film thickness of 97.2 ± 0.8 Å and its top surface roughness 2.1 ± 1.6 Å. A surface oxide layer of 22 ± 1 Å and roughness 7 ± 5 Å exists on top of the Nb.

lens produces a circular spot 100 μm in diameter, while the latter one focuses light in a rectangle of approximately 100 μm$\times$1 cm. The larger beam size allows for less incident intensity for a given laser power, thus reducing sample heating which could drive the superconductor into the normal state. The collimated Raman-scattered light is passed through a polarizer to select the appropriate polarization, then passed through a depolarizer to eliminate polarization effects in the monochromator, and then through a holographic filter to remove light scattered at the original laser frequency. Finally, the light is guided through an *f*-matched spherical lens into a triple spectrometer or a single monochromator. The former allows for a higher resolution and lower signal-to-noise ratio, while the latter has a higher throughput, thus allowing the use of shorter collection times and lower laser power, important for the low temperature experiments. A liquid nitrogen cooled CCD is used as a detector with a resulting spectral resolution of $1.5-3.0$ cm^{-1}, depending on the excitation wavelength used. A calibrated spectrum of an Ar pen-lamp is used for calibration of the CCD wavelength axis. Low temperature measurements are performed in an optical immersion cryostat with four optical windows.

The sample temperature is monitored with a manufacturer-calibrated Si diode. Independent temperature monitoring is done by measuring the four-probe sample resistance, and comparing it to the measurements performed before and after the Raman experiment in another cryostat, using a germanium resistor thermometer with manufacturer's calibration.

III. MATERIALS AND THEIR CHARACTERIZATION

A. Niobium

An x-ray diffraction $\Theta-2\Theta$ scan for a typical Nb film grown on sapphire is presented in Fig. 1. The only peak that is not related to the sapphire substrate is at 38.46° and corresponds to (110) Nb. This single-peak diffraction pattern indicates a highly textured film with no secondary phases or orientations observable. Scanning electron microscopy (SEM) detects no features on a 100-Å-thick Nb film, indicating smoothness to the measurement resolution of 30 Å.

In order to characterize Nb/sapphire and Nb/InAs surface and interface quality (roughness and materials interdiffusion), low-angle x-ray reflectivity measurements are employed. Experimental results and modeling of Nb/InAs sample AR050595-B are shown in Fig. 2. Here, the reflectivity is plotted as a function of the wave-vector transfer. For a single uniform layer of material, the value of $1/\Delta q$, where Δq is the period of the oscillations, is proportional to the film thickness, and the roughness of the film is determined from the maximum wave-vector transfer at which oscillations are observed. In order to deduce thickness and roughness of all layers of the sample, an accurate fit to a standard reflectivity model,[25] is plotted as a line in Fig. 2. This best fit for this film yields an InAs substrate roughness of 1.4 ± 1.0 Å, a Nb film thickness of 97.2 ± 0.8 Å and a top surface roughness of 2.1 ± 1.6 Å. A surface oxide layer of 22 ± 1 Å and roughness 7 ± 5 Å exists on the top surface of the Nb.

The electronic mean-free path of the Nb thin films is calculated using the Drude conductivity $\sigma=ne^2\tau/m$, substituting l/v_F for τ, where l is the mean free path, and v_F is the Fermi velocity. The temperature-independent part of bulk resistivity ρ_{0_b} can be expressed as

$$\rho_{0_b}=\frac{mv_F}{ne^2l_0}, \tag{1}$$

where l_0 is a zero-temperature mean free path. When the thickness of the film d is reduced to a value comparable to the mean free path, boundary scattering reduces the effective mean free path,[26,27] and for $d\ll l$, the temperature-independent part of resistivity ρ_0 of such thin film yields

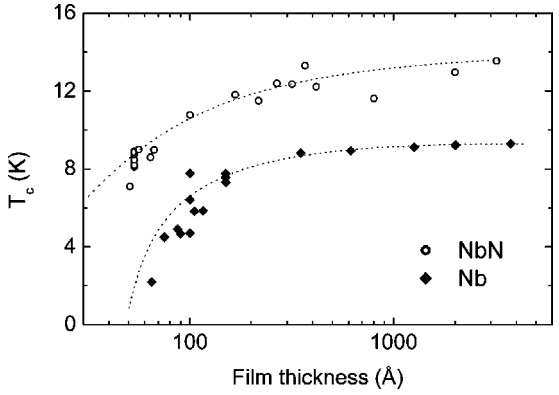

FIG. 3. Critical temperature of Nb and NbN films as a function of film thickness. A gradual reduction in T_c is observed between 2000 and 100 Å with a dramatic reduction in T_c for films thinner than 100 Å (after Refs. 9,10).

$$\frac{\rho_0}{\rho_{0_b}} = \frac{4}{3}\frac{l_0/d}{\ln(l_0/d)}, \tag{2}$$

where ρ_{0_b} is defined by Eq. (1). Using a Nb carrier concentration of $n=5.56\times10^{22}$ cm^{-3} (Ref. 28), and a mean field value for the Fermi velocity of $v_F=0.3\times10^8$ cm/s (Refs. 29–31), Eq. (1) yields $\rho_0 l_0=1.9\times10^{-6}\mu\Omega$ cm^2. The values for l_0, obtained for 50-100 Å-thick films are typically 20–30 Å less than the measured film thickness, which is attributed at least partially to the formation of an oxide surface layer. Some reduction in the crystalline quality of the films is also likely at these lower thicknesses.

Nb films thicker than 2000 Å, grown on either sapphire or InAs, exhibit the bulk Nb T_c of 9.2 K, with 20–50 mK transition widths. As the film thickness is decreased from 2000 Å, a gradual reduction in T_c is observed down to 100 Å, with a dramatic reduction in T_c for films thinner than 100 Å as shown in Fig. 3 (Ref. 9). The residual resistivity ratio of Nb films RRR$=R_{300\,K}/R_{10\,K}$ is also reduced from 50–150 for 4000-Å-thick films to 3–5 for 100-Å-thick films. Studies of conductivity and superconducting energy gap of our superconducting thin Nb films by far infrared and microwave techniques are published elsewhere.[32]

B. Niobium nitride

Experiments were also performed with NbN_x replacing Nb, because there are several advantages to using this compound superconductor over the metallic one. First, NbN_x exhibits an intrinsically higher T_c, typically 13–17 K, dependent upon x. This allows a broader range of measurements below T_c, since our optical cryostat is limited to 1.2 K. Second, the carrier concentration of NbN_x is typically several times lower than that of Nb. This leads to a lower skin depth, so a NbN_x film has a higher optical transmittance than a Nb film of the same thickness. As a result, in comparison to Nb, thicker NbN_x films can be used in optical experiments, where the light is sent through the superconducting film, before optical extinction occurs, so systems with higher T_c can be probed. Finally, the coherence length of NbN_x, typically 20 Å, is much shorter compared to that of Nb, thus providing less T_c reduction with decreasing thickness. This is shown in Fig. 3, where for any given film thickness, the T_c of a NbN_x thin film is higher than that of a Nb thin film.

In the normal state, NbN_x films have a small negative slope of the $R(T)$ curve. The residual resistivity ratios RRR$=R_{300\,K}/R_{15\,K}$, for these films ranges between 0.85 and 0.95, with the highest values corresponding to thicker films. The room temperature resistivity ranges between 90 and 150 $\mu\Omega$ cm for thickest films, and increases to 250–300 mΩ cm for 50–60-Å-thick films.

C. Indium arsenide

InAs is a direct gap III-V semiconductor with a zincblende structure. The minimum of the conduction band (G_6) is situated in the center of the Brillouin zone. The value of the direct gap[33] is 356 meV at 300 K, and 418 meV at 4.2 K . Near the conduction band minimum, the energy dispersion $E(k)$, is isotropic but nonparabolic. The effective electron mass is therefore a scalar, and depends strongly on the electron concentration. The value of the effective electron mass ranges from 0.02 m_e to 0.12 m_e, for concentrations of 10^{16} and 10^{20} cm^{-3}, respectively, where m_e is the free electron mass.

A metal, deposited on a semiconductor surface, can influence the band bending. There are several different theoretical models for the electronic band bending at semiconductor/metal interfaces, the first ones being proposed by Schottky[34] and Mott.[35] Systematic experimental studies of the influence of the metal coverage on the band bending of *n*-InSb and *n*- and *p*-InAs were done by Corden.[36,37] Evaporation of Au, Al, Sn, and In on the surface of these semiconductors resulted in band bending which, as measured by the intensity of the LO mode, was found to be different in each case, and could not be directly correlated with the metal work function values. An extensive review of experimental studies of band bending modification for different surface coverages is given by Guerts.[14] There is still no single theoretical model which accounts for all of the observed near-surface electronic properties, and which would predict the band configuration when an arbitrary metal and an arbitrary semiconductor are joined.

We observe changes in the near surface band structure of highly doped (10^{19} cm^{-3}) *n*-InAs due to sputter-deposited metal, Ar-ion etching, oxidation and chemical passivation of the surface.[16,17] The processing of the InAs for our proximity effect experiments is optimized to minimize modification of the CAR at all steps of the sample preparation process.

There are two types of optical phonon modes in InAs: transverse (TO) and longitudinal (LO). The frequencies of these two modes ω_{TO} and ω_{LO} are related by the Lyddane-Sachs-Teller relation $\omega_{TO}/\omega_{LO}=[\varepsilon(\infty)/\varepsilon(0)]^{1/2}$, where $\varepsilon(0)$ and $\varepsilon(\infty)$ are the zero and high-frequency dielectric constants of the medium. The shift in TO phonon frequency is caused by the interaction with the ionic mean field. The frequency of the TO mode does not depend on the presence of free carriers, as predicted by group theory for a zincblende insulator.[38] The LO mode is affected by the presence of the free carriers at concentrations higher than

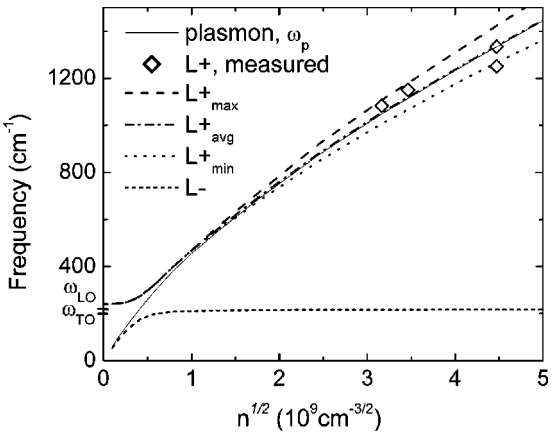

FIG. 4. Phonon and plasmon mode frequencies as a function of the square root of the carrier concentration, calculated using Eqs. (3) and (4). Three curves for the L_+ mode, L_+max, L_+min, and L_+avg, are calculated using the maximum, minimum, and average values for the effective mass, respectively, obtained experimentally by different methods (Refs. 33,40) and ranging from $0.02m_e$, for the undoped InAs, to $0.07m_e-0.10m_e$, for $n=10^{19}$ cm^{-3}.

$\sim 10^{17}$ cm^{-3} (Ref. 39). Any free carriers in the material will produce a plasmon mode, whose frequency ω_p increases with carrier concentration n as

$$\omega_p^2=\frac{4\pi e^2 n}{\varepsilon(\infty)m^*}, \tag{3}$$

where m^* is the effective mass of the free carriers. The LO phonon and plasmon can couple, which results in the *coupled plasmon-phonon modes* L_- and L_+ at frequencies Ω^- and Ω^+, respectively. The frequency of these coupled modes is given by[14]

$$(\Omega^{\pm})^2=\frac{1}{2}[(\omega_p{}^2+\omega_{LO}{}^2) \pm\sqrt{(\omega_p{}^2-\omega_{LO}{}^2)^2+4\omega_p{}^2(\omega_{LO}{}^2-\omega_{TO}{}^2)}]. \tag{4}$$

The frequencies of these two modes are plotted according to Eq. (4) in Fig. 4 as a function of the square root of the carrier density. The plasmon frequency ω_p is also plotted in Fig. 4. A deviation of ω_p from pure square root dependence is due to the effective mass dependence on the carrier concentration. For undoped InAs, m^* is consistently quoted at $0.02m_e$, where m_e is the free electron mass. The value of m^* increases with doping and quotes in the literature for it become less consistent.[33,40] For $n=10^{19}$ cm^{-3}, m^* reaches values of $0.07m_e-0.10m_e$. The plasmon frequency is plotted using a linearly interpolated average values of m^*. For the L_+ mode, three curves, $L_{+\max}$, $L_{+\min}$, and $L_{+\text{avg}}$, are calculated using the maximum, minimum, and average experimental values for the effective mass, respectively,[33,40] and linear interpolation.

At low carrier concentration the L_- mode follows ω_p and asymptotically approaches the TO mode frequency ω_{TO} with

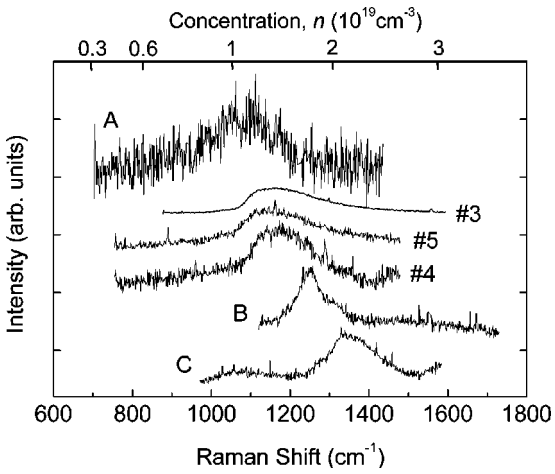

FIG. 5. L_+ plasmon-phonon coupled mode for different InAs wafers: three bulk-grown wafers (Nos. 3, 4, 5) with the nominal concentration of 1.2×10^{19} cm^{-3}, and three MBE-grown InAs wafers, one nominally at $n=1\times10^{19}$ cm^{-3} (A), and two (B and C) nominally at $n=2\times10^{19}$ cm^{-3} (EB0308, EB0272, EB0269, respectively). The top axis provides the corresponding concentration values as estimated from Eq. (4) and Fig. 4.

increasing n. The L_+ mode matches the LO mode frequency ω_{LO} at low carrier concentration and at higher n follows the plasmon frequency, ω_p.

Since the frequency of the L_+ mode shows a strong and well-defined dependence on carrier concentration at sufficiently high doping levels, it can serve as a tool to determine the carrier concentration. Raman spectra in the region of the L_+ mode for different InAs wafers with different concentrations are presented in Fig. 5 The following wafers are tested: three different bulk-grown wafers (Nos. 3, 4, 5) with the nominal concentration of 1.2×10^{19} cm^{-3}, and three different MBE-grown InAs wafers, one nominally at $n=1\times10^{19}$ cm^{-3} (EB0308), and two (EB0272 and EB0269) nominally at $n=2\times10^{19}$ cm^{-3}. We also plot the experimentally determined ω_{L_+} as a function of $n^{1/2}$ in Fig. 4, and the excellent agreement with the calculated dependence indicates that the nominal concentrations agree with the measured concentrations. This finding is especially important for the MBE-grown semiconductors, because these materials have several different layers with different doping levels, and therefore, their doping level cannot be simply measured using the Hall effect, as is usually done for bulk semiconductors.

The uncertainty in the LO mode wave vector within the CAR δk_{LO} is governed by the Heisenberg uncertainty principle $\delta k_{LO} d_{CAR} \geqslant 1$. Since at $n\sim10^{18}-10^{19}$ cm^{-3}, d_{CAR} is 30–50 Å, the uncertainty in k_{LO} becomes larger than the Thomas-Fermi screening wave vector. As a result, the longitudinal phonon mode is no longer effectively screened by electrons in the CAR, and can be observed at the original LO frequency in highly doped InAs. Thus, in the $x(y,z)\bar{x}$ geometry of the Raman measurements presented here, the L_- and L_+ modes of highly doped n-InAs arise primarily from the bulk, and the LO mode arises from the near-surface CAR.

Intensities of the L_- and LO modes can serve as a tool to

TABLE I. Intensity ratios of the LO phonon mode to the coupled phonon-plasmon mode based on sampling depth for several wavelengths. Resonance is with the E_1 gap of InAs (after Refs. 10,11).

	Probe wavelength (nm)	Sampling depth (Å)	Intesnsity ration I_{LO}/I_{L_-}
resonant at 4 K	457.9	75	1.14
nonresonant at 4 K	488.0	92	0.71
resonant at 300 K	496.5	96	0.80
nonresonant at 300 K	514.5	133	0.58

study the strength of the band bending and to measure the width of the CAR.[14] This is possible because the optical sampling depth is finite, so that with increasing band bending, the intensity of the L_- mode decreases, while that of the LO mode increases. The increase of the CAR width therefore constitutes an increase of the volume where the LO mode exists. The intensity ratio of the LO and L_- mode in a highly doped InAs depends on the CAR width d_{CAR}:[14]

$$I_{\mathrm{LO}}I_{L_-}=\frac{R_{\mathrm{LO}}}{R_{L_-}}[\exp(2\alpha d_{\mathrm{CAR}})-1], \tag{5}$$

where R_{LO} and R_{L_-} are the effective Raman scattering tensor elements for the LO and L_- modes, respectively. The probing depth $1/2\alpha$ (α is the extinction coefficient), defined as half of the light penetration depth (skin depth), depends on the light frequency ω and the dielectric constant ε. The LO intensity I_{LO} from the CAR can be related to the LO intensity of an undoped sample I_{L_-}:[14]

$$I_{\mathrm{LO}}=I_{L_-}[1-\exp(-2\alpha d_{\mathrm{CAR}})]. \tag{6}$$

An example of the LO/L_- test done on bulk-grown single crystals of highly doped n^+InAs ($n=1.2\times10^{19}$ cm^{-3}), and undoped InAs ($n=1.8\times10^{16}$ cm^{-3}) is presented in Table I. Raman measurements are performed in the $x(y,z)\bar{x}$ geometry, using all four available wavelengths at room temperature and at 4 K. The E_1 gap at the Brillouin zone boundary in InAs is 2.62 eV at room temperature and 2.50 eV at 4 K. Therefore all laser frequencies are close to the E_1-gap resonance. The Raman signal is significantly larger for the lines that are nearly at the InAs E_1 optical resonance 457.9 nm (at 2–10 K) and 496.5 nm (at 300 K), than for those lines that are farther away from the resonance: 488.0 and 514.5 nm, respectively. The intensity ratios as well as the probing depth estimated from the extinction coefficient for all four laser wavelengths used are presented in Table I. The CAR width d_{CAR} for the same highly doped InAs ($n=1.2\times10^{19}$ cm^{-3}) is found to be 35 ± 3 Å.

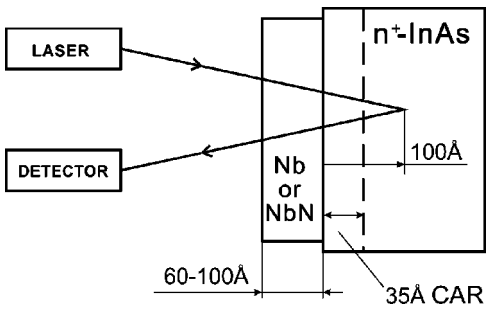

FIG. 6. Sketch of the Raman measurements used for detection of the superconducting proximity effect, performed in near-backscattering geometry. The light from an argon ion laser, operated at four wavelengths 457.9, 488, 496.5, and 514.5, passes through a thin (60–100Å) superconducting film (Nb or NbN) and scatters from the near-surface region of InAs. Raman spectra arising from LO, L_-, and L_+ modes are observed at temperatures above and below T_c.

IV. EXPERIMENTAL RESULTS

A. Raman measurements of the proximity effect at the SN interface

The studies of the superconducting proximity effect by Raman scattering are done using 60–100-Å-thick superconducting films (Nb or NbN) sputter deposited on a single crystal of highly doped (1.2×10^{19} cm^{-3}) n-InAs as shown schematically in Fig. 6. Raman measurements are performed in the $x(y,z)\bar{x}$ geometry using a probe wavelength of 457.9 nm, near resonant to the E_1 gap at 4K.

For Nb/InAs samples, two modes LO and L_- are measured at two temperatures 10 and 2 K, which are above and below T_c of Nb/InAs, respectively. As described above, the LO phonon mode is associated with the near surface charge accumulation region (CAR), while the L_- plasmon-phonon coupled mode arises predominantly from the bulk. The magnitude of the total light scattered is different at these two temperatures, because at 2 K the sample is immersed in superfluid He. For this reason, the absolute mode intensity can not be used for temperature dependent comparisons. Therefore, the ratio of the intensities of the LO and L_- modes is used. It is observed that this ratio I_{LO}/I_{L_-} measured at 2 and 10 K, is enhanced below T_c (2.5–5 K) by up to 40% (Fig. 7). This observed change in the phonon spectrum is reversible upon cycling through the superconducting transition temperature. At cryogenic temperatures, the laser power can be high enough to heat the sample by several degrees. This allows temperature cycling to be done by two different methods: by changing the He-bath temperature and by changing the laser power. In both cases, the change of the sample resistance at the superconducting transition is monitored.

Raman measurements are also done on the bare InAs, off the Nb film. No change in the Raman peak intensities with temperature between 2 and 10 K is observed in this case.

Raman measurements are also performed on identical samples, except that no surface etch is done prior to Nb deposition, i.e., when the native oxide layer, estimated to be about 30-Å thick, is present at the interface between the superconductor and the semiconductor. No spectroscopic

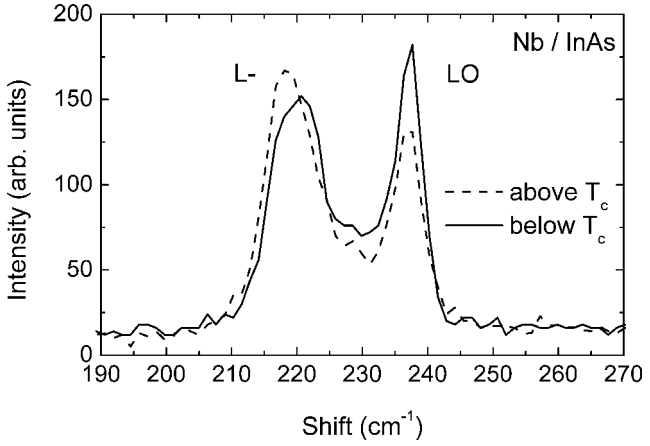

FIG. 7. Raman spectrum for Nb on InAs: LO phonon (arising from the CAR) and L_- (primarily from scattering in the bulk) phonon-plasmon coupled modes are shown as taken at 10 and 2 K, above and below $T_c = 4.5$ K, respectively. Note the ratio of the intensities I_{LO}/I_{L_-} is enhanced below T_c.

change is observed in this material over the same temperature range. This confirms that the intensity change only occurs when the Nb is in a good electrical contact with the InAs.

It is important to note that Nb is not optically active at these frequencies, so it does not participate in the Raman scattering process itself. Thus, we conclude that the intensity change occurs in the InAs being in good electrical contact with the Nb, and, therefore, this change is due to a superconducting proximity effect.

Results, similar to those observed with Nb/InAs are also observed for the NbN/InAs system (Fig. 8).

No change in the relative intensity of LO and L_- modes is observed above 10 K. At temperatures much higher than 10 K, the temperature-dependent E_1 gap increases, hence changing the resonance conditions for the laser probe. Having the laser probe frequency farther away from the resonance leads to a smaller Raman signal.

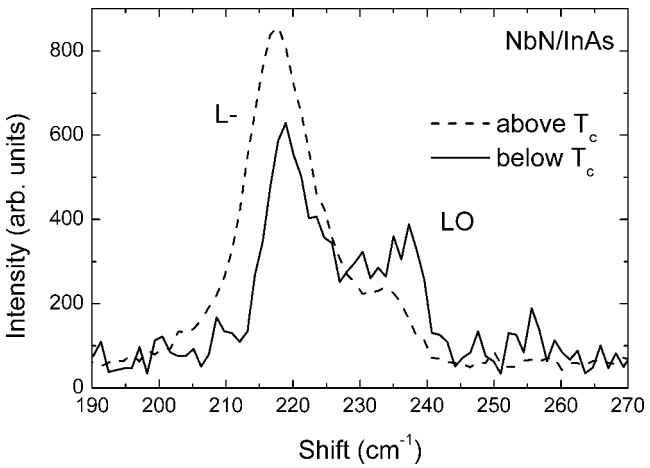

FIG. 8. Raman spectrum for NbN on InAs: LO phonon (arising from the CAR) and L_- (primarily from scattering in the bulk) phonon-plasmon coupled modes are shown as taken at 10 and 2 K, above and below $T_c = 8$ K, respectively. Note the ratio of the intensities I_{LO}/I_{L_-} is enhanced below T_c.

The observation of this proximity effect is very sensitive to the interface quality, and to the InAs material itself. It is mentioned that the surface oxide is removed by a gentle *in situ* Ar-ion etch. Our studies[16,17] show that an increase in either the etch time or the ion energy causes significant damage to the InAs surface, thus reducing the intensity of the LO-mode. When the LO peak is weak compared to the L_- (e.g., when it is just a small shoulder on L_-, and its height is less than 10% of that of the L_- mode), it is difficult to measure any change in the intensity, and therefore, to perform studies using the LO mode. We also observe that the surface damage due to Nb sputtering can reduce the intensity of the LO mode, reducing it so that the LO-phonon peak appears as just a shoulder on the L_- peak. The near surface band structure of the MBE-grown InAs is more sensitive to the Ar-ion etching and Nb deposition than that of the single-crystal InAs. This may be due to the differences in the near-surface structure of the InAs caused by differences in the initial treatment of the tested InAs samples. Bulk-grown single-crystal InAs is cut and polished, while the surface of the epitaxially grown InAs is either capped with As (which is removed thermally *in situ* just prior to Nb deposition) or not treated at all. No measurable spectroscopic change upon crossing T_c is observed using MBE-grown InAs.

B. L_+ mode for Nb/InAs samples

It is suggested that the charge density in the near surface region of InAs can change upon the superconducting transition. Since the center frequency of the L_+ mode is very sensitive to the carrier concentration, measurements of the L_+ mode at temperatures above and below the T_c provide a measure of any change in the charge density. No changes in either the position or the strength of the L_+ peak are observed between 2 and 10 K, within the available experimental resolution. Although the L_+ mode peak is more than 100 cm^{-1} wide and its intensity is more than 20 times smaller than that of the L_- and LO modes, our measurements allow changes in carrier concentration as small as 5×10^{17} cm^{-3} to be measured. However, because of the large uncertainty in the k-vector due to a small size of the CAR, the L_+ mode in the CAR may be damped by the single-electron excitations, and in this case the signal from the L_+ in the CAR may not be detected. Therefore, concentration changes within the CAR cannot be reliably measured by the L_+ center frequency.

Measurements of the intersubband absorption resonance in a Nb/InAs/AlSb quantum well have been reported by Eckhause *et al.*[41] This resonance is sensitive to the electron density in the InAs. No change in absorption with the temperature decreased below T_c was found by that group, indicating that no significant charge transfer occurs at the superconducting transition.

V. DISCUSSION

A change in the intensity of the LO phonon and L_- plasmon-phonon coupled mode of the InAs is observed upon

crossing the superconducting critical temperature T_c. This change is only observed when the InAs is in good electrical contact with the superconductor Nb or NbN. These changes in the Raman spectrum cannot be due to the onset of the superconductivity in the superconductor alone. First, since a superconducting transition in a zero applied magnetic field is a second-order transition, and therefore, is not accompanied by a volume change, it does not cause changes in the crystal lattice to produce strain on the InAs. Second, the changes in the electronic structure of the Nb or NbN upon crossing T_c, i.e., the superconducting gap opening, are negligible on the energy scale of the Raman scattering experiment. The Nb superconducting gap in our films is 1.5 meV or smaller (1.7–3.3 meV for NbN_x), while all other energy scales are much larger: The phonon energy is ~29 meV, the Fermi energy estimated for this high level of doping is ~280 meV from the bottom of the conduction band, the direct optical gap of InAs is ~418 meV, and the probing light frequency corresponds to ~2.5 eV. Thus, the observed effect can only be due to the change in the near surface electronic properties of the InAs upon the superconducting transition, and we conclude that it is a superconducting proximity effect.

The observed change may be attributed to one or several of the following processes occurring in the surface charge accumulation region: (1) increase in the scattering volume of the LO phonon due to an increase in the CAR width, (2) decrease in the probing length due to an increase in the extinction coefficient, (3) increase in the carrier concentration, (4) phase correlation of charge carriers, (5) change in the conductivity of the InAs, and (6) influence on the electron-phonon interaction in the InAs. Each is briefly discussed below.

The scattering intensity of the LO phonon with respect to that of the L_- mode would increase, if the scattering volume of the LO-phonon increases due to an increase in the width of the CAR. Such a change in the CAR width can be caused, for example, by a change in the *SN* interface states that determine the band bending.

An increase of the extinction coefficient would lead to a decrease in the light penetration depth, thus reducing the probing depth. The width of the CAR, the region of the LO mode existence, is smaller than the probing depth, so the entire CAR is always probed. Therefore the intensity of the LO mode should remain the same. At the same time, the sampled volume of the bulk, from which L_- predominantly originates, is reduced. Since the volume of the bulk probed, compared to the volume of the CAR probed, is reduced, the intensity of the LO mode relative to that of the L_- mode is increased.

Additional charges leaking into InAs from Nb would increase the carrier concentration in the InAs. Thus, the number of the carriers that can participate in Raman scattering process is increased. Then the Raman cross-section would be certainly increased in InAs, and, the LO mode intensity would be enhanced, since the increase in n would happen primarily in the CAR. There is no obvious mechanism for carrier concentration increase, and no such change was detected within our experimental resolution.

Below the superconducting transition temperature, electrons in the InAs CAR participate in the Andreev reflection, therefore developing some degree of phase correlation. The fraction of electrons undergoing Andreev reflection may be estimated by taking into account the differences in the effective masses and Fermi momenta of Nb and InAs. Assuming a clean interface, we follow the method suggested by Blonder.[42] Considering an electron as a plane wave, and matching the boundary conditions, we estimate the probability for Andreev reflection for electrons near the Fermi surface to be $A=[1+(1-r)^2/2r]^{-2}$, where r is the Fermi velocity ratio for the Nb and InAs. The mean field value for the Fermi velocity of Nb is $v_F=0.3\times10^8$cm/s (Refs. 29–31). For InAs ($n=1.2\times10^{19}$ cm^{-3}, $m_{eff}=0.08m_e$), we find $v_F=\hbar(3\pi^2n)^{1/2}/m_{eff}=1.03\times10^8$ cm/s. In this case we can estimate the ideal probability for Andreev reflection to be 29%. Proximity-induced electron coherence certainly increases the low-frequency conductivity of the near-interface region of the Nb. The effect on the conductivity at frequencies much higher than the superconducting energy gap is very small. However, at frequencies very close to an optical gap, such as the E_1 gap in our case, the dielectric constant ε changes very rapidly with frequency. The derivative $d\varepsilon/d\omega$, and therefore $d\sigma/d\omega$, has a very large value. As a consequence, a tiny shift in the resonance frequency can result in a significant change in optical properties of InAs, including the light penetration depth. For this reason, a small effect of the superconductor-induced electron correlation on the high-frequency conductivity can be amplified due to resonance effects in the vicinity of the E_1 optical resonance in InAs, resulting in significantly larger optical absorption and a small probing depth.

It may be possible that the interaction between the longitudinal phonons and the electrons changes due to the presence of the superconductor, changing the Raman tensor. It is worth noting that the strength of the LO phonon-electron interaction can be estimated from the $\omega_{LO}-\omega_{L_-}$ difference, and is about 18 cm^{-1}, that is, ~2.25 meV for these InAs samples. This value is comparable to the energy scale of the electron-phonon interaction in the superconductor defined as twice the superconducting energy gap 2Δ. For bulk Nb, $2\Delta\approx3$ meV (see Ref. 32, and references therein), and for NbN, 2Δ ranges from 3.4 to 6.6 meV (see, e.g., Refs. 43–45), depending on the material quality. Thus, it is at least energeticallyu feasible for the opening of a superconducting gap to affect electron-phonon coupling in InAs.

When this paper was in preparation, we learned about the theoretical investigation of a *SINIS* system, where *I* is a very thin barrier that can be due to a Fermi velocity mismatch at the inferface.[46] Nikolić *et al.* calculate the distribution of the electron density at temperatures surrounding T_c of the system. When the electron densities in *S* and *N* differ by two orders of magnitude, they observe a change in the electron concentration in the normal layer when the temperature is decreased from $1.8T_c$ to $0.09T_c$. This theoretical model addresses a system with parameters similar to those of our samples, except that we have a superconductor only on one side. Currently, due to the limitations initially set in the

model, it cannot predict the resulting changes in the CAR parameters.

The superconducting proximity effect is observed by optical measurements. A change in the electronic properties of the near-surface charge accumulation region of InAs with the superconducting transition is reported. A few possibilities for the mechanism of this effect are suggested. Further studies, both experimental and theoretical, are required to find the exact mechanism responsible for this observed effect.

ACKNOWLEDGMENTS

The authors would like to thank W. L. Feldmann for his talented technical assistance. We also thank I. K. Robinson for initial x-ray reflectivity measurements on our films and G. Kuhler for help in establishing NbN growth procedure. Fruitful discussions with G. Blumberg, E. Burnstein, M. Cardona, Y.-C. Chang, J. K. Freericks, P. M. Goldbart, D. J. Van Harlingen, Yu. Lyanda-Geller, M. V. Klein, D. M.-T. Kuo, D. Maslov, B. K. Nikolić, A. Pinczuk, R. R. Ramazashvili, J. A. Sauls, A. Shnirman, and M. Turlakov are acknowledged. We gratefully acknowledge support from the United States Department of Energy through Materials Research Laboratory (Grant No. DEFG02-96ER45439) (I.V.R., A.C.A., L.H.G., T.A.T., J.F.D., P.W.B., J.F.K.), and from the United States Department of Energy through Midwest Superconductivity Consortium (MISCON) (Grant No. DE FG02-90ER45427) and the NSF (Grant No. DMR 96-23827) (S.W.H., P.F.M.). SEM, XRD, XPS, and RBS materials characterizations were performed at the Center for Microanalysis of Materials and Microfabrication Center at Frederick Seitz Materials Research Laboratory, University of Illinois at Urbana-Champaign (Grant No. DE FG02-96ER45439). Sandia is a multiprogram laboratory operated by Sandia Corporation, a Lockheed Martin company, for the United States Department of Energy under Contract No. DE-AC04-94AL85000.

*Present address: Department of Physics, UCSD, 9500 Gillman Dr., La Jolla, CA 92093-0319.

†Present address: SPAWAR Systems Center, 53560 Hull Street, San Diego, CA 92152.

‡Present address: Advanced Micro Devices, 5204 E. Ben White Blvd. M/S 612, Austin, TX 78741.

§Present address: Shell Oil, Houston, TX.

**Present address: Chemical Sciences Division, Lawrence Berkeley National Laboratory, Berkeley, CA 94720.

[1] A.F. Andreev, Sov. Phys. JETP **19**, 1228 (1964).

[2] P. de Gennes, *Superconductivity in Metals and Alloys* (Benjamin, New York, 1966).

[3] G. Deutcher and P. DeGennes, in *Superconductivity*, edited by R. Parks (Marcel Dekker, New York, 1969), pp. 1005–1034.

[4] G. Blonder, M. Tinkham, and T. Klapwijk, Phys. Rev. B **25**, 4515 (1982).

[5] A. Kastalsky, A. Kleinsasser, L. Greene, R. Bhat, F. Milliken, and K. Harbison, Phys. Rev. Lett. **67**, 3026 (1991).

[6] B. van Wees, P. de Vries, P. Magnèe, and T. Klapwijk, Phys. Rev. Lett. **69**, 510 (1992).

[7] I. Marmorkos, C. Beenakker, and M. Jalabert, Phys. Rev. B **48**, 2811 (1993).

[8] A. Volkov, Physica C **235-240**, 1869 (1994).

[9] I.V. Roshchin, Ph.D. thesis, Physics Department, University of Illinois at Urbana-Champaign, Urbana, 2000.

[10] L.H. Greene, A.C. Abeyta, I.V. Roshchin, I.K. Robinson, J.F. Dorsten, T.A. Tanzer, and P.W. Bohn, Proc. SPIE **2696/1**, 215 (1996).

[11] L.H. Greene, J.F. Dorsten, I.V. Roshchin, A.C. Abeyta, T.A. Tanzer, G. Kuchler, W.L. Feldmann, and P.W. Bohn, Czech. J. Phys. **46**, 3115 (1996).

[12] L.H. Greene, J.F. Dorsten, I.V. Roshchin, A.C. Abeyta, T.A. Tanzer, W.L. Feldmann, and P.W. Bohn, Czech. J. Phys. **46**, 741 (1996).

[13] A. Kleinsasser and W. Gallagher, in *Superconducting Devices*, edited by S. Ruggiero and D. A. Rudman (Academic Press, San Diego, 1990), pp. 325–372.

[14] J. Guerts, Surf. Sci. **18**, 1 (1993).

[15] A. Many, Y. Goldstein, and N. Grover, *Semiconductor Surfaces* (North-Holland, Amsterdam, 1965).

[16] T.A. Tanzer, P.W. Bohn, I.V. Roshchin, L.H. Greene, and J.F. Klem, Appl. Phys. Lett. **75**, 2794 (1999).

[17] T.A. Tanzer, P.W. Bohn, I.V. Roshchin, and L.H. Greene, J. Vac. Sci. Technol. B **18**, 144 (2000).

[18] J.F. Dorsten, J.E. Maslar, and P.W. Bohn, Appl. Phys. Lett. **66**, 1755 (1995).

[19] L.A. Farrow, C.J. Sandroff, and M.C. Tamargo, Appl. Phys. Lett. **51**, 1931 (1987).

[20] J.E. Maslar, J.F. Dorsten, P.W. Bohn, S. Agarwala, I. Adesida, C. Caneau, and R. Bhat, J. Vac. Sci. Technol. B **13**, 988 (1995).

[21] B. Boudbart, B. Prevot, and C. Schwab, Appl. Surf. Sci. **50**, 295 (1991).

[22] P.D. Wang, M.A. Foad, C.M. Sotomayor-Torres, S. Thoms, M. Watt, R. Cheung, C.D.W. Wilkinson, and S.P. Beaumont, J. Appl. Phys. **71**, 3754 (1992).

[23] G. Abstreiter, M. Cardona, and A. Pinczuk, in *Light Scattering in Solinds*, edited by M. Cardona (Springer-Verlag, Berlin, 1984), Vol. 4, p. 542.

[24] T.A. Tanzer, Ph.D. thesis, Chemistry Department, University of Illinois at Urbana-Champaign, 1999.

[25] L.G. Parratt, Phys. Rev. B **95**, 359 (1954); S.K. Sinha, E.B. Sirota, S. Garoff, and H.B. Stanley, *ibid.* **38**, 2297 (1988); P.F. Miceli in *Semiconductor Interfaces, Microstructures and Devices: Properties and Applications*, edited by Z.C. Feng (IOP, Bristol, 1993), p. 87.

[26] G.T. Meaden, *Electrical Resistance of Metals, The Cryogenics Monograph Series* (Plenum, New York, 1965).

[27] K. Fuchs, Proc. Cambridge Philos. Soc. **34**, 100 (1938).

[28] N.W. Ashcroft and N.D. Mermin, *Solid States Physics* (Saunders College Publishing, Orlando, 1976).

[29] C. Kittel, *Introduction to Solid State Physics* 6th ed. (Wiley, New York, 1986).

[30] H.W. Weber, E. Seidl, C. Laa, E. Schachinger, M. Prohammer, A. Junod, and D. Eckert, Phys. Rev. B **44**, 7585 (1991).

[31] L.F. Mattheiss, Phys. Rev. B **1**, 373 (1970).

[32] A.V. Pronin, M. Dressel, A. Pimenov, A. Loidl, I.V. Roshchin, and L.H. Greene, Phys. Rev. B **57**, 14 416 (1998).

[33] O. Madelung, *Intrinsic Properties of III-V Materials* (Springler-Verlag, Berlin, 1991).
[34] W. Schottky, Naturwissenschaften **26**, 843 (1938).
[35] N. Mott, Proc. Cambridge Philos. Soc. **34**, 568 (1938).
[36] P.S. Corden, A. Pinczuk, and E. Burstein, Proc. 10th Intl. Conf. Phys. Semicond., edited by S.P. Keller, J. C. Hensel, and F. Stern (1970) (unpublished), p. 739.
[37] P.S. Corden, Ph.D. thesis, University of Pennsylvania, Philadelphia, 1971.
[38] R. Loudon, Adv. Phys. **13**, 423 (1964).
[39] A. Mooradian and A. McWhorter, Phys. Rev. Lett. **19**, 849 (1967).
[40] *Semiconductors: Group IV Elements and III-V Compounds*, edited by O. Madelung, Data in science and technology (Springer-Verlag, Berlin, 1991).
[41] T.A. Eckhause, S. Tsujino, K.W. Lehnert, E. Gwinn, S.J. Allen, M. Thomas, and H. Kroemer, Appl. Phys. Lett. **76**, 215 (1999).
[42] G.E. Blonder, Harvard University Technical Report No. 19, 1982 (unpublished).
[43] S. Isagawa, J. Appl. Phys. **52**, 921 (1981).
[44] L. Chen, S.M. Green, and H.L. Luo, J. Appl. Phys. **64**, 145 (1986).
[45] E.A. Antonova, D.R. Dzhuraev, G.P. Motulevich, and V.A. Sukhov, Zh. Eksp. Teor. Fiz. **80**, 2426 (1981).
[46] B.K. Nikolić, J.K. Freericks, and P. Miller, Phys. Rev. B **65**, 064529 (2002).